Switching on a two-dimensional time-harmonic scalar wave in the presence of a diffracting edge

D. P. Hewett[*,a,1], J. R. Ockendon[b], D. J. Allwright[a]

[a] *Oxford Centre for Industrial and Applied Mathematics (OCIAM), Mathematical Institute, 24–29 St. Giles, Oxford OX1 3LB, UK*

[b] *Oxford Centre for Collaborative Applied Mathematics (OCCAM), Mathematical Institute, 24–29 St. Giles, Oxford OX1 3LB, UK*

Abstract

This paper concerns the switching on of two-dimensional time-harmonic scalar waves. We first review the switch-on problem for a point source in free space, then proceed to analyse the analogous problem for the diffraction of a plane wave by a half-line (the 'Sommerfeld problem'), determining in both cases the conditions under which the field is well-approximated by the solution of the corresponding frequency domain problem. In both cases the rate of convergence to the frequency domain solution is found to be dependent on the strength of the singularity on the leading wavefront. In the case of plane wave diffraction at grazing incidence the frequency domain solution is immediately attained along the shadow boundary after the arrival of the leading wavefront. The case of non-grazing incidence is also considered.

Key words: Diffraction, Time Domain, Frequency Domain, Limiting Amplitude Principle.

[*]Corresponding author

Email address: d.p.hewett@reading.ac.uk (D. P. Hewett)

[1]Present address: Department of Mathematics, University of Reading, Whiteknights, PO Box 220, Reading RG6 6AX, UK

1. Introduction

When a time-harmonic source is switched on, one might expect that as the time since the source was switched on increases, the resulting time-dependent wave field should gradually approach the solution of a corresponding frequency domain problem, in which the source has 'always been on'. The existence of this limiting solution is often referred to as the Limiting Amplitude principle, and it is well-known that this principle holds in the case of scattering by smooth obstacles of fields due to smooth source distributions (see e.g. [1, 2, 3]).

The case where the scatterer possesses boundary singularities has not been studied in such detail, although in a recent publication [4] the Limiting Amplitude principle has been proved for the scattering of an incoming plane wave by a wedge. However, the analysis in [4] did not extend to the calculation of the rate of convergence to the frequency domain solution, and this is the problem we address in this paper, in the special case where the scatterer is a half-line.

Assuming that the half-line scatterer is along $y = 0$, $x \geq 0$, the time-dependent diffraction problem we consider is

$$\frac{\partial^2 \Phi}{\partial t^2} - c_0^2 \nabla^2 \Phi = 0, \qquad 0 < r < \infty, \quad 0 < \theta < 2\pi, \tag{1}$$

where (r, θ) are the usual polar coordinates, along with the rigid (Neumann) boundary condition

$$\frac{\partial \Phi}{\partial \theta} = 0, \qquad 0 < r < \infty, \quad \theta \in \{0, 2\pi\}, \tag{2}$$

and a suitable prescription of the 'switched on' incident plane wave. For ease of presentation we initially restrict our attention to the simplest case, where the wave is incident from the direction $\theta_0 = 0^+$, with

$$\Phi = H(\pi - \theta) G(t + x/c_0), \qquad t < 0, \tag{3}$$

before discussing the general case in section 3.3. Here, and in what follows, $H(\cdot)$ represents the Heaviside unit step function. The source function G governing the profile of the incident wave is assumed to take the form

$$G(t) = H(t) e^{-i\omega t}, \tag{4}$$

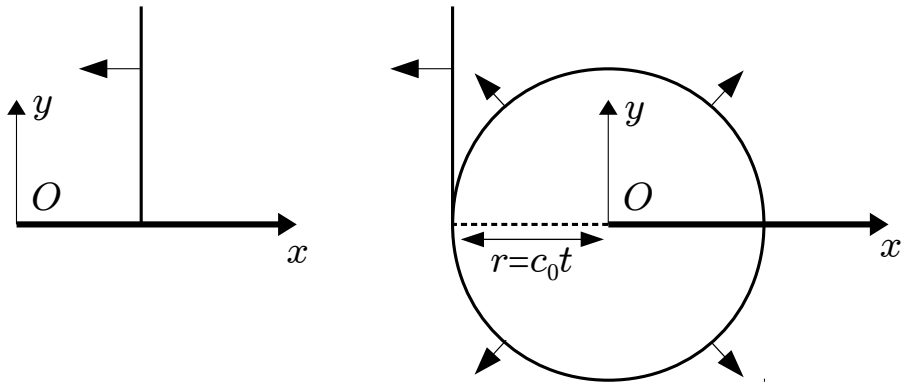

(a) $t < 0$ (b) $t > 0$

Figure 1: Wavefront configurations.

for some angular frequency $\omega > 0$. This choice of source function implies that the incident wave reaches the diffracting edge at time $t = 0$. A diagram showing the resulting wavefront configurations can be found in Figure 1.

The wave function Φ is complex-valued, with $\mathrm{Re}\,[\Phi]$ and $\mathrm{Im}\,[\Phi]$ representing the responses to the incident waves with source functions $H(t)\cos\omega t$ and $-H(t)\sin\omega t$, respectively. Note that, in contrast to [4], where the profile of the incoming plane wave is assumed to be smooth, we consider here the case where the incident wave is switched on 'instantaneously', with a jump discontinuity across the leading wavefront, either in the incident field (as is the case for $\mathrm{Re}\,[\Phi]$) or in its derivative in the direction of incidence (as is the case for $\mathrm{Im}\,[\Phi]$).

For large time we shall show, with error bounds, that $\mathrm{Re}\,[\Phi]$ and $\mathrm{Im}\,[\Phi]$ are well-approximated by the real and imaginary parts, respectively, of $\Phi_{\mathrm{freq}} = e^{-i\omega t}\phi$, where the 'limiting amplitude' ϕ is the solution of the corresponding frequency domain problem (the classical 'Sommerfeld problem'), comprising the Helmholtz equation

$$\left(\nabla^2 + k^2\right)\phi = 0, \qquad 0 < r < \infty, \quad 0 < \theta < 2\pi, \tag{5}$$

where $k = \omega/c_0$, the boundary condition

$$\frac{\partial\phi}{\partial\theta} = 0, \qquad 0 < r < \infty, \quad \theta \in \{0, 2\pi\}, \tag{6}$$

and the assumption that

$$\phi - H(\pi - \theta)e^{-ikx} \tag{7}$$

should satisfy an outgoing radiation condition for $\theta \neq \pi$.

Before analysing this diffraction problem, we consider first the simpler problem of switching on a point source in two-dimensional free space. In this case, the time-dependent problem is

$$\frac{\partial^2 \Phi}{\partial t^2} - c_0^2 \nabla^2 \Phi = \delta(\mathbf{x})G(t), \qquad \mathbf{x} \in \mathbf{R^2}, \tag{8}$$

with G defined as in (4) and $\Phi = 0$ for $t < 0$. Again the function Φ is complex-valued, with $\mathrm{Re}\,[\Phi]$ and $\mathrm{Im}\,[\Phi]$ representing the responses to the source functions $H(t)\cos\omega t$ and $-H(t)\sin\omega t$, respectively. The corresponding frequency domain problem for the limiting amplitude ϕ comprises the Helmholtz equation

$$\left(\nabla^2 + k^2\right)\phi = -\frac{1}{c_0^2}\delta(\mathbf{x}), \qquad \mathbf{x} \in \mathbf{R^2}, \tag{9}$$

and an outgoing radiation condition at infinity.

Our approach to both problems follows the same pattern. We first express the solution Φ of the time-dependent problem as the convolution of the source function G and the (known) solution Φ_δ to the appropriate 'impulse response' problem, in which the source function is $\delta(t)$. We then analyse the short time behaviour of Φ (i.e. immediately after the arrival of the leading wavefront), which is governed by the short time behaviour of the source function G. Finally, we consider the long time behaviour, defining

$$\delta\Phi := \Phi_{\mathrm{freq}} - \Phi, \tag{10}$$

and proceeding to determine the conditions under which[2]

$$\delta_{\mathrm{R}} := \frac{\mathrm{Re}[\delta\Phi]}{|\Phi_{\mathrm{freq}}|} \to 0, \tag{11}$$

$$\delta_{\mathrm{I}} := \frac{\mathrm{Im}[\delta\Phi]}{|\Phi_{\mathrm{freq}}|} \to 0, \tag{12}$$

[2]Note that (11) and (12) represent convergence relative to $|\Phi_{\mathrm{freq}}| = |\phi|$, the local amplitude of oscillation of $\mathrm{Re}\,[\Phi_{\mathrm{freq}}]$ and $\mathrm{Im}\,[\Phi_{\mathrm{freq}}]$. Thus if (11) and (12) hold $\mathrm{Re}\,[\Phi]$ and $\mathrm{Im}\,[\Phi]$ are well-approximated by $\mathrm{Re}[\Phi_{\mathrm{freq}}]$ and $\mathrm{Im}[\Phi_{\mathrm{freq}}]$, respectively, in the sense that for a given observation point, the graphs of the functions (as functions of t) look alike.

and also the timescale over which the convergence occurs. In particular, we find that for both problems the convergence is nonuniform with respect to the point of observation, and that the rate of convergence is dependent on the strength of the singularity on the leading wavefront.

2. Switching on a point source in two-dimensional free space

The solution Φ of (8) for any source function G is given by the convolution of G with the impulse response function Φ_δ, i.e. the fundamental solution of the wave equation,

$$\Phi_\delta = \frac{H(t - r/c_0)}{2\pi c_0^2 \sqrt{t^2 - (r/c_0)^2}}. \tag{13}$$

With G defined as in (4) this gives

$$\Phi = \frac{H(t - r/c_0)}{2\pi c_0^2} \int_{r/c_0}^{t} \frac{e^{-i\omega(t-s)}}{\sqrt{s^2 - (r/c_0)^2}}\, ds, \tag{14}$$

which can be conveniently rewritten as

$$\Phi = \frac{H(\xi)}{2\pi c_0^2} \int_0^{\xi} \frac{e^{i(s-\xi)}}{\sqrt{s(s+2\eta)}}\, ds, \tag{15}$$

in terms of the nondimensional variables $\xi = \omega t - kr = \omega(t - r/c_0)$ and $\eta = kr = \omega r/c_0$, and a new dimensionless integration variable. Note that ξ represents 2π times the number of periods of oscillation since the arrival of the leading wavefront (which arrives at time $t = r/c_0$), and η represents 2π times the number of wavelengths between the observation point and the source.

2.1. Behaviour near the leading wavefront

The behaviour of Φ near the leading wavefront is found by approximating (15) in the limit as $\xi \to 0^+$. Since (15) can be written, for $0 < \xi < 2\eta$, as

$$\Phi = \frac{1}{2\pi c_0^2 \sqrt{2\eta}} \int_0^{\xi} \frac{(1 + i(s-\xi) + ...)}{\sqrt{s}} \left(1 - \frac{s}{4\eta} + \dots\right) ds, \tag{16}$$

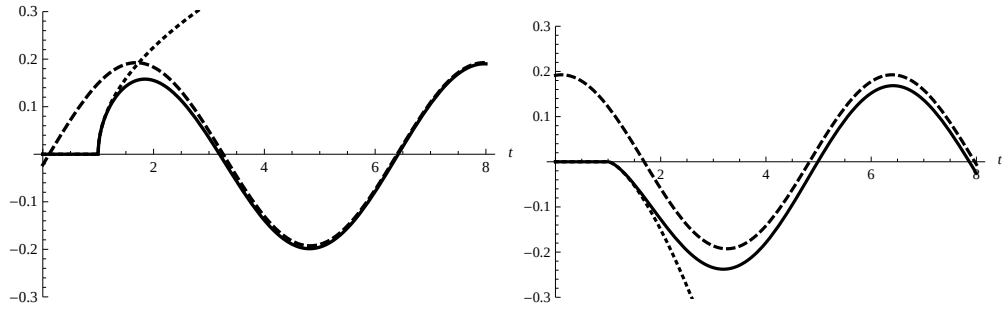

(a) Re[Φ] (b) Im[Φ]

Figure 2: Switching on a time-harmonic point source in two-dimensional free space. Comparison of Φ (solid curves), Φ_{freq} (dashed curves) and the wavefront approximations (17) and (18) (dotted curves). Parameter values are $\omega = 1$, $c_0 = 1$, $r = 1$, so that the leading wavefront arrives at $t = 1$.

we see that

$$\text{Re}[\Phi] \sim \frac{H(\xi)}{\sqrt{2}\pi c_0^2\sqrt{\eta}}\xi^{1/2}, \qquad \xi \to 0,\ \xi \ll \eta, \tag{17}$$

$$\text{Im}[\Phi] \sim -\frac{\sqrt{2}H(\xi)}{3\pi c_0^2\sqrt{\eta}}\xi^{3/2}, \qquad \xi \to 0,\ \xi \ll \eta. \tag{18}$$

Note the difference in the strength of the singularity in $\text{Re}\,[\Phi]$ and $\text{Im}\,[\Phi]$ on the leading wavefront: $\text{Re}\,[\Phi]$ is continuous across $\xi = 0$, with $\frac{\partial \text{Re}[\Phi]}{\partial \xi}$ posessing an inverse square root singularity; $\text{Im}\,[\Phi]$ is continuously differentiable across $\xi = 0$, with $\frac{\partial^2 \text{Im}[\Phi]}{\partial \xi^2}$ posessing an inverse square root singularity.

2.2. Convergence to the frequency domain solution

The frequency domain solution in this case is

$$\Phi_{\text{freq}} = \frac{ie^{-i\omega t}}{4c_0^2}H_0^{(1)}(\eta), \tag{19}$$

where $H_0^{(1)}(\eta) = J_0(\eta) + iY_0(\eta)$ is the zero-order Hankel function of the first kind. Plots of Φ, Φ_{freq} and the wavefront approximations (17) and (18) as functions of t, with the other parameters fixed, can be found in Figure 2. In the case considered in Figure 2 the leading wavefront arrives at $t = 1$.

For t close to 1, $\mathrm{Re}[\Phi]$ and $\mathrm{Im}[\Phi]$ are well-approximated by (17) and (18). As time progresses (i.e. as $\xi \to \infty$), $\mathrm{Re}[\Phi]$ and $\mathrm{Im}[\Phi]$ gradually approach $\mathrm{Re}[\Phi_{\mathrm{freq}}]$ and $\mathrm{Im}[\Phi_{\mathrm{freq}}]$, respectively. Interestingly, the convergence of $\mathrm{Re}[\Phi]$ appears to be faster than that of $\mathrm{Im}[\Phi]$, and we will comment further on this observation shortly.

There are various possible approaches to the study of the large time behaviour of wave functions such as (15), for example, by using the Cagniard/de Hoop representation in terms of the Laplace transformation (cf. [5]). Our approach is to consider direct asymptotics as $\xi \to \infty$ in (15), which will require different expansions in different regions of physical space.

We begin by noting that, as one might expect from naïvely sending $\xi \to \infty$ in (15), the frequency domain solution (19) can be written as (cf. [6], 9.1.24)

$$\Phi_{\mathrm{freq}} = \frac{1}{2\pi c_0^2} \int_0^\infty \frac{e^{i(s-\xi)}}{\sqrt{s(s+2\eta)}}\, ds. \tag{20}$$

Hence

$$\delta\Phi = \frac{1}{2\pi c_0^2} \int_\xi^\infty \frac{e^{i(s-\xi)}}{\sqrt{s(s+2\eta)}}\, ds, \qquad \xi > 0, \tag{21}$$

and repeated integration by parts gives the asymptotic behaviour

$$\mathrm{Re}[\delta\Phi] \sim \frac{(\xi+\eta)}{2\pi c_0^2 (\xi(\xi+2\eta))^{3/2}} \left(1 + O\left(\frac{1}{\xi^2}\right)\right), \qquad \xi \to \infty, \tag{22}$$

$$\mathrm{Im}[\delta\Phi] \sim \frac{1}{2\pi c_0^2 \sqrt{\xi(\xi+2\eta)}} \left(1 + O\left(\frac{1}{\xi^2}\right)\right), \qquad \xi \to \infty, \tag{23}$$

uniformly for all $\eta > 0$.

This implies that,

- for $\eta = O(1)$ but bounded away from zero (e.g. for kr fixed),

$$\delta_{\mathrm{R}} = O\left(\frac{1}{\xi^2}\right), \qquad \xi \to \infty,\ \eta = O(1), \tag{24}$$

$$\delta_{\mathrm{I}} = O\left(\frac{1}{\xi}\right), \qquad \xi \to \infty,\ \eta = O(1), \tag{25}$$

  since $|\Phi_{\mathrm{freq}}| = O(1)$ in this regime. Hence, as observed in Figure 2, the convergence of $\mathrm{Re}[\Phi]$ is indeed faster than that of $\mathrm{Im}[\Phi]$.

- For $\eta \ll 1$ (i.e. for observation points close to the source) we have (cf. [6], 9.1.12 and 9.1.13)

$$\Phi_{\text{freq}} \sim \frac{e^{-i\omega t}}{2\pi c_0^2}\left(-\log(\eta) + (\log 2 - \gamma) + \frac{i\pi}{2} + O\left(\eta^2|\log\eta|\right)\right), \quad \eta \ll 1, \tag{26}$$

and combining (26) with (22) and (23) gives

$$\delta_{\text{R}} = O\left(\frac{1}{\xi^2|\log\eta|}\right), \qquad \xi \to \infty,\ \eta \ll 1, \tag{27}$$

$$\delta_{\text{I}} = O\left(\frac{1}{\xi|\log\eta|}\right), \qquad \xi \to \infty,\ \eta \ll 1. \tag{28}$$

In fact, the assumption that $\eta \ll 1$ is enough to give convergence even when ξ is not large. For $\xi > 2\eta$ we may expand the integrand in (21) to give

$$\delta\Phi = \frac{1}{2\pi c_0^2}\int_\xi^\infty \frac{e^{i(s-\xi)}}{s}\left(1 - \frac{\eta}{s} + \ldots\right) ds, \tag{29}$$

so that

$$\delta\Phi \sim \frac{1}{2\pi c_0^2}\int_\xi^\infty \frac{e^{i(s-\xi)}}{s}\, ds, \qquad \eta \ll \xi. \tag{30}$$

In particular, when $\xi = O(1)$, but bounded away from zero, (11) and (12) hold with

$$\delta_{\text{R}},\, \delta_{\text{I}} = O\left(\frac{1}{|\log\eta|}\right), \qquad \xi = O(1),\ \eta \ll 1. \tag{31}$$

When $\xi \ll 1$ we have

$$\text{Re}\left[\int_\xi^\infty \frac{e^{i(s-\xi)}}{s}\, ds\right] \sim -\log\xi + O(1), \qquad \xi \ll 1, \tag{32}$$

$$\text{Im}\left[\int_\xi^\infty \frac{e^{i(s-\xi)}}{s}\, ds\right] \sim \frac{\pi}{2} + O\left(\xi|\log\xi|\right), \qquad \xi \ll 1, \tag{33}$$

so that with $\eta \ll \xi \ll 1$, (11) and (12) hold with

$$\delta_{\mathrm{R}} = O\left(\frac{|\log \xi|}{|\log \eta|}\right), \qquad \eta \ll \xi \ll 1, \tag{34}$$

$$\delta_{\mathrm{I}} = O\left(\frac{1}{|\log \eta|}\right), \qquad \eta \ll \xi \ll 1. \tag{35}$$

For completeness we remark that with $\eta \ll 1$ the estimate (35) (and hence (12)) holds even for $\xi = O(\eta)$, as can be shown by combining the expansions (26) and (16).

- For $\eta \gg 1$ (i.e. for observation points far from the source) we have (cf. [6])

$$\Phi_{\mathrm{freq}} \sim \frac{ie^{-i(\xi+\pi/4)}}{4c_0^2}\sqrt{\frac{2}{\pi\eta}}\left(1 - \frac{i}{8\eta} + \dots\right), \qquad \eta \gg 1, \tag{36}$$

and combining (36) with (22) and (23) gives

$$\delta_{\mathrm{R}} = O\left(\frac{1}{\xi^{3/2}}\right), \qquad 1 \ll \eta,\ \xi = O(\eta), \tag{37}$$

$$\delta_{\mathrm{I}} = O\left(\frac{1}{\sqrt{\xi}}\right), \qquad 1 \ll \eta,\ \xi = O(\eta), \tag{38}$$

and

$$\delta_{\mathrm{R}} = O\left(\frac{\sqrt{\eta}}{\xi^2}\right), \qquad 1 \ll \eta \ll \xi, \tag{39}$$

$$\delta_{\mathrm{I}} = O\left(\frac{\sqrt{\eta}}{\xi}\right), \qquad 1 \ll \eta \ll \xi. \tag{40}$$

We can summarise by saying that a receiver that is switched on many periods after the passage of the leading wavefront will register the frequency domain solution

- with algebraic error (24, 25) when the receiver is a few wavelengths from the source;
- with slightly smaller error (27, 28) when the receiver is closer to the source than a wavelength;

- with larger error (37, 38) or (39, 40) when the receiver is many wavelengths from the source.

We now analyse the diffraction problem using a similar approach.

3. Switching on a plane wave incident on a half-line

As in the point source case, the solution Φ of the time-dependent problem (1)-(3) is given by the convolution of the source function G with the appropriate impulse response function Φ_δ. In the diffraction case, Φ_δ is given by[3]

$$\Phi_\delta = H(\pi-\theta)\delta\left(t+x/c_0\right) - \operatorname{sgn}(\pi-\theta)\frac{H(t-r/c_0)}{2\pi}\frac{\sqrt{r(1+\cos\theta)}}{\sqrt{c_0t-r}(t+\frac{r}{c_0}\cos\theta)}, \tag{41}$$

which can be obtained, for example, by differentiating with respect to t the response to an incident step discontinuity (source function $G(t) = H(t)$), given by (cf. [7], p. 123, or [8])

$$\Phi_{\text{step}} = H(\pi-\theta)H(t+x/c_0) - \operatorname{sgn}(\pi-\theta)\frac{H(t-r/c_0)}{\pi}\arctan\left[\sqrt{\frac{c_0t-r}{r(1+\cos\theta)}}\right]. \tag{42}$$

With G defined as in (4) this gives

$$\begin{aligned}\Phi = {} & H(\pi-\theta)H(t+x/c_0)e^{-i(\omega t+kx)} \\ & - \operatorname{sgn}(\pi-\theta)\frac{H(t-r/c_0)}{2\pi}\sqrt{r(1+\cos\theta)}\int_{r/c_0}^{t}\frac{e^{-i\omega(t-s)}}{\sqrt{c_0s-r}(s+\frac{r}{c_0}\cos\theta)}\,ds,\end{aligned} \tag{43}$$

or

$$\Phi = H(\pi-\theta)H(\xi^{\text{inc}})e^{-i\xi^{\text{inc}}} - \operatorname{sgn}(\pi-\theta)\frac{H(\xi)\sqrt{\eta}}{2\pi}\int_0^{\xi}\frac{e^{i(s-\xi)}}{\sqrt{s}(s+\eta)}\,ds, \tag{44}$$

[3] In (41), and subsequently, the value of $H(0)$ is assigned to be $1/2$. The expression (41) is then analytic in $0 < r < c_0t$.

in terms of the nondimensional variables $\xi^{\rm inc} = \omega t + kx = \omega(t + x/c_0)$, $\xi = \omega t - kr = \omega(t - r/c_0)$ and $\eta = kr(1 + \cos\theta) = \omega r/c_0(1 + \cos\theta)$. Note that $\xi^{\rm inc}$ and ξ represent 2π times the number of periods of oscillation that have elapsed since the arrivals of the incident and diffracted wavefronts respectively. For ωt fixed, curves of constant $\xi^{\rm inc}$ and ξ are parallel lines and circles centered at the origin respectively. The variable η provides a measure of how close the observation point is to the shadow boundary $\theta = \pi$ of the frequency domain problem. Curves of constant η are parabolae with focus at the origin and axis along the shadow boundary (which corresponds to $\eta = 0$). The limit $\eta \to \infty$ represents the regime in which ray theory is valid for the frequency domain problem.

3.1. Behaviour close to the leading wavefront

In the line-of-sight (LOS) region $\theta < \pi$ the leading wavefront is the incident wavefront $\xi^{\rm inc} = 0$. Provided that $r > c_0 t$ we have

$$\mathrm{Re}[\Phi] \sim H(\xi^{\rm inc}), \qquad \xi^{\rm inc} \to 0, \tag{45}$$

$$\mathrm{Im}[\Phi] \sim -H(\xi^{\rm inc})\,\xi^{\rm inc}, \qquad \xi^{\rm inc} \to 0, \tag{46}$$

so that $\mathrm{Re}[\Phi]$ undergoes a jump discontinuity across $\xi^{\rm inc} = 0$ and $\mathrm{Im}[\Phi]$ is continuous across $\xi^{\rm inc} = 0$, with $\frac{\partial \mathrm{Im}[\Phi]}{\partial \xi^{\rm inc}}$ undergoing a jump discontinuity.

In the non-line-of-sight (NLOS) region $\theta > \pi$ the first term in (44) is not present, and the leading wavefront is the diffracted wavefront $\xi = 0$. Expanding

$$\Phi = \frac{H(\xi)\sqrt{\eta}}{2\pi} \int_0^{\xi} \frac{1 + i(s - \xi) + \dots}{\sqrt{s}(s + \eta)}\, ds, \tag{47}$$

we find that

$$\mathrm{Re}[\Phi] \sim \frac{H(\xi)\sqrt{\eta}}{2\pi} \int_0^{\xi} \frac{1}{\sqrt{s}(s + \eta)}\, ds = \frac{H(\xi)}{\pi} \arctan\sqrt{\frac{\xi}{\eta}}, \qquad \xi \to 0, \tag{48}$$

$$\mathrm{Im}[\Phi] \sim \frac{H(\xi)\sqrt{\eta}}{2\pi} \int_0^{\xi} \frac{s - \xi}{\sqrt{s}(s + \eta)}\, ds = \frac{H(\xi)}{\pi} \left(\sqrt{\eta\xi} - (\eta + \xi) \arctan\sqrt{\frac{\xi}{\eta}} \right), \quad \xi \to 0, \tag{49}$$

and provided that $\xi \ll \eta$ we can further expand to obtain

$$\mathrm{Re}[\Phi] \sim \frac{H(\xi)}{\pi\sqrt{\eta}}\xi^{1/2}, \qquad \xi \to 0,\ \xi \ll \eta, \tag{50}$$

$$\mathrm{Im}[\Phi] \sim -\frac{2H(\xi)}{3\pi\sqrt{\eta}}\xi^{3/2}, \qquad \xi \to 0,\ \xi \ll \eta. \tag{51}$$

Note that in both $\mathrm{Re}[\Phi]$ and $\mathrm{Im}[\Phi]$ the strength of the singularity on the diffracted wavefront is weaker than that on the incident wavefront by half a power of ξ, which is a general principle of edge diffraction (see [9] for further discussion).

In the LOS region $\theta < \pi$, (50) and (51) imply that for $\xi^{\mathrm{inc}} > 0$

$$\mathrm{Re}[\Phi] \sim \cos\xi^{\mathrm{inc}} - \frac{H(\xi)}{\pi\sqrt{\eta}}\xi^{1/2}, \qquad \xi \to 0,\ \xi \ll \eta, \tag{52}$$

$$\mathrm{Im}[\Phi] \sim -\sin\xi^{\mathrm{inc}} + \frac{2H(\xi)}{3\pi\sqrt{\eta}}\xi^{3/2}, \qquad \xi \to 0,\ \xi \ll \eta. \tag{53}$$

Curves on which $\zeta = \xi/\eta$ is constant have the equation

$$r = \frac{\frac{c_0 t}{\zeta+1}}{1 + (\frac{\zeta}{\zeta+1})\cos\theta}, \tag{54}$$

which describes a family of ellipses, whose axes all lie on the shadow boundary $\theta = \pi$. Their foci are at $(0,0)$ and $\left(-\frac{c_0 t}{1+1/2\zeta}, 0\right)$, and they have eccentricity $\frac{\zeta}{\zeta+1}$, so that each ellipse intersects the circle $r = c_0 t$ at exactly one point, namely $r = c_0 t$, $\theta = \pi$. The region of validity of the approximations (50)-(53) can therefore be thought of as being a thin annular region $0 < \xi \ll 1$, minus the interior of a thin ellipse $\zeta \ll 1$.

3.2. Convergence to the frequency domain solution

The solution of the frequency domain diffraction problem is (e.g. [10, p556])

$$\Phi_{\mathrm{freq}} = \frac{e^{-i(\omega t + kx + \pi/4)}}{\sqrt{\pi}} \int_{-\sqrt{2kr}\cos\frac{\theta}{2}}^{\infty} e^{is^2}\, ds. \tag{55}$$

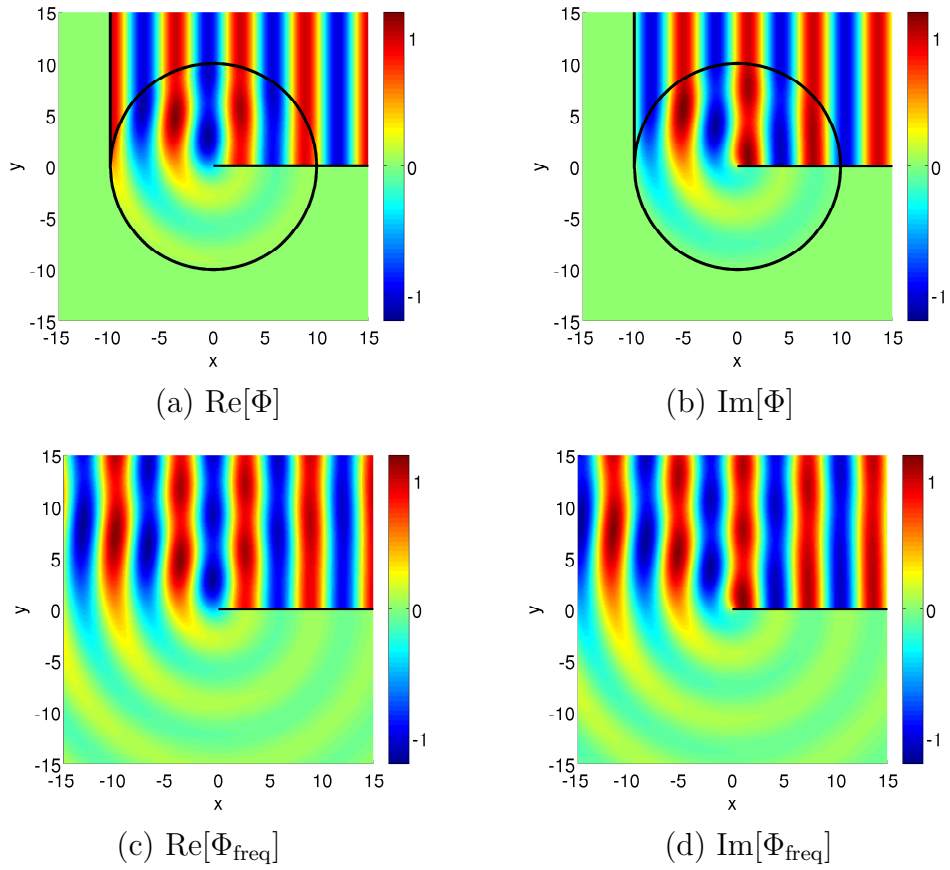

(a) Re[Φ] (b) Im[Φ]

(c) Re[Φ_{freq}] (d) Im[Φ_{freq}]

Figure 3: Diffraction of a switched on plane wave by a half-line. The half-line and the incident and diffracted wavefronts have been highlighted. Parameter values are $\theta_0 = 0^+$, $t = 10$, $\omega = 1$, $c_0 = 1$.

Typical plots of Φ and Φ_{freq} for fixed t can be found in Figure 3. Plots of Φ, Φ_{freq} and the wavefront approximations (50)-(53) as functions of t, with the other parameters fixed, can be found in Figure 4.

In Figures 4(a)-(d) the receiver is located in the NLOS region $\theta > \pi$, where the leading wavefront is the diffracted wavefront, which in this case arrives at $t = 1$. The local behaviour near this wavefront is governed by the approximations (50) and (51). In Figures 4(e)-(h) the receiver is located in the LOS region $\theta < \pi$, where the leading wavefront is the incident wavefront, which in this case arrives at $t = -\cos\theta$. The local behaviour near this wavefront is governed by the approximations (45) and (46). At time $t = 1$ the

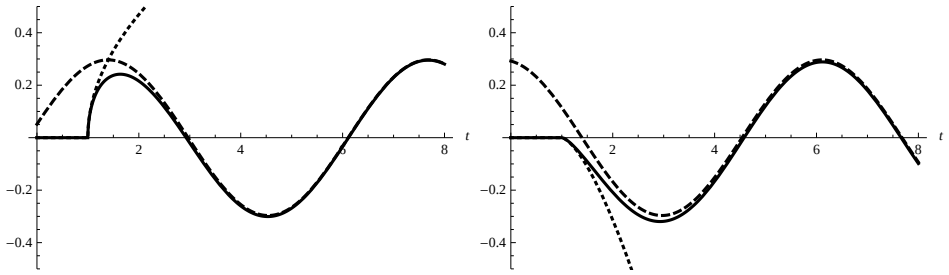

(a) Re[Φ], $\theta = \pi + 1$ (b) Im[Φ], $\theta = \pi + 1$

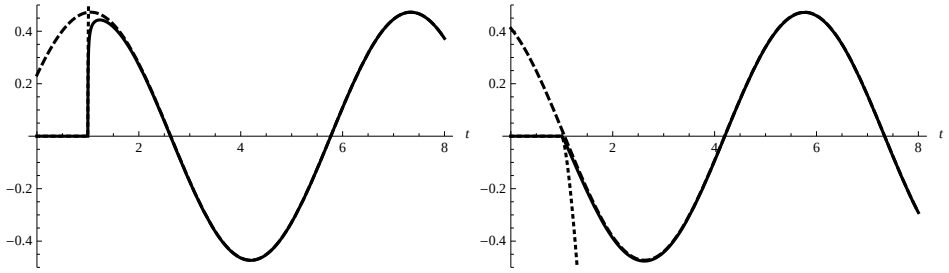

(c) Re[Φ], $\theta = \pi + 0.1$ (d) Im[Φ], $\theta = \pi + 0.1$

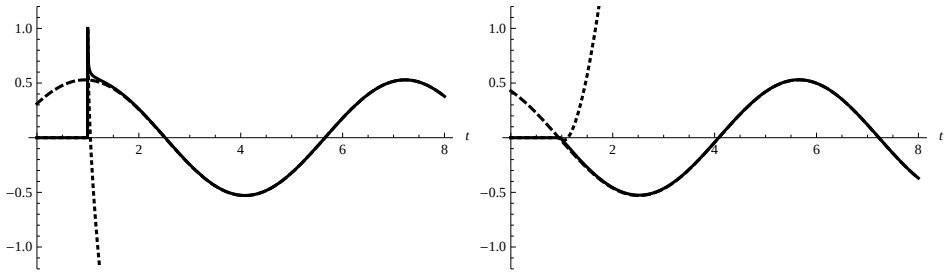

(e) Re[Φ], $\theta = \pi - 0.1$ (f) Im[Φ], $\theta = \pi - 0.1$

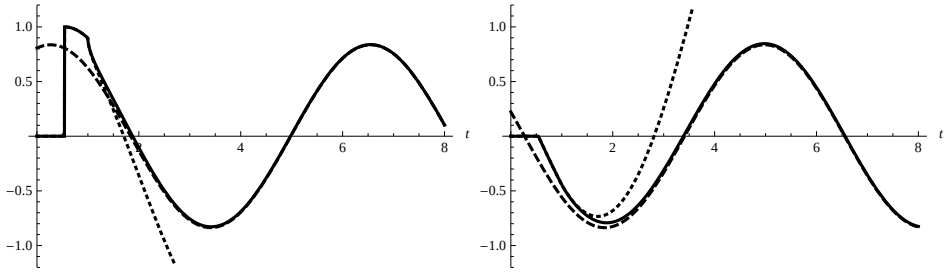

(g) Re[Φ], $\theta = \pi - 1$ (h) Im[Φ], $\theta = \pi - 1$

Figure 4: Comparison of Φ (solid curves), Φ_{freq} (dashed curves) and the wavefront approximations (50)-(53) (dotted curves). Magnified versions of plots (c)-(f) can be found in Figure 5. Parameter values are $\theta_0 = 0^+$, $\omega = 1$, $c_0 = 1$, $r = 1$.

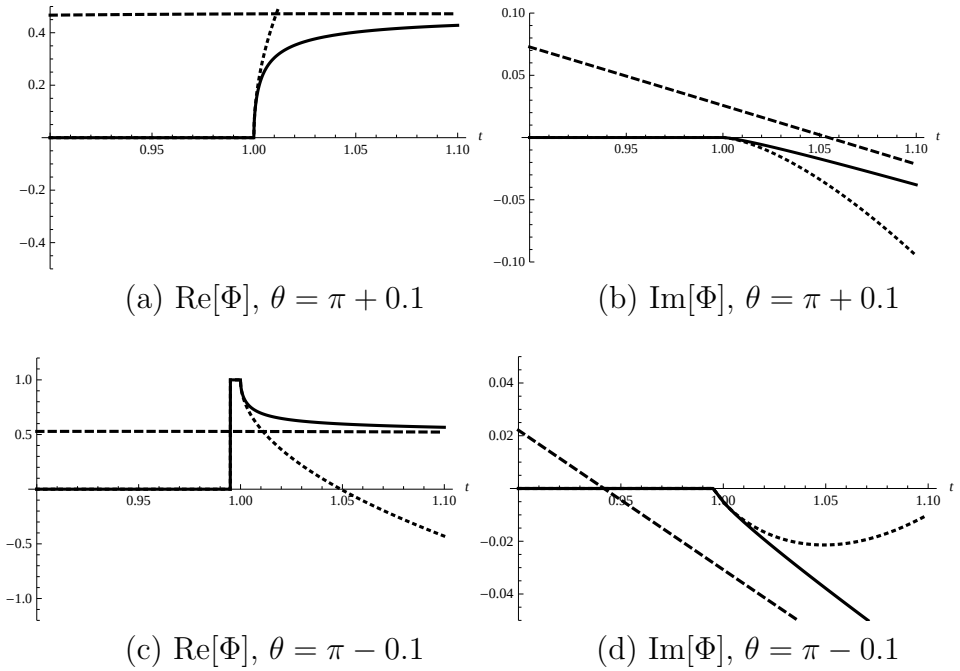

(a) Re[Φ], $\theta = \pi + 0.1$ (b) Im[Φ], $\theta = \pi + 0.1$

(c) Re[Φ], $\theta = \pi - 0.1$ (d) Im[Φ], $\theta = \pi - 0.1$

Figure 5: Magnified version of Figure 4(c)-(f).

diffracted wavefront arrives, and the local behaviour is governed by (52) and (53). Magnified versions of Figures 4(c)-(f) showing this local behaviour can be found in Figure 5.

As time progresses we observe that Re[Φ] and Im[Φ] gradually approach the appropriate frequency domain solutions. As in the point source case, the convergence of Re[Φ] appears to be faster than that of Im[Φ]. Also, the convergence of both Re[Φ] and Im[Φ] appears to be faster for $\theta = \pi \pm 0.1$ than for $\theta = \pi \pm 1$, an indication that the convergence is not uniform with respect to θ. This is confirmed by plotting $|\delta_{\mathrm{R}}|$ and $|\delta_{\mathrm{I}}|$ as a function of position, for fixed t, which we do in Figures 6(a) and 6(b).

We remark that the concentric rings observed in Figures 6(a) and 6(b) in the region $r > c_0 t$ are due to the zeros of the diffracted component of Φ_{freq}, and do not represent regions of convergence to the frequency domain solution. Indeed, from this point on we shall restrict our attention almost exclusively to the behaviour of δ_{R} and δ_{I} *inside* the diffracted region $r < c_0 t$.

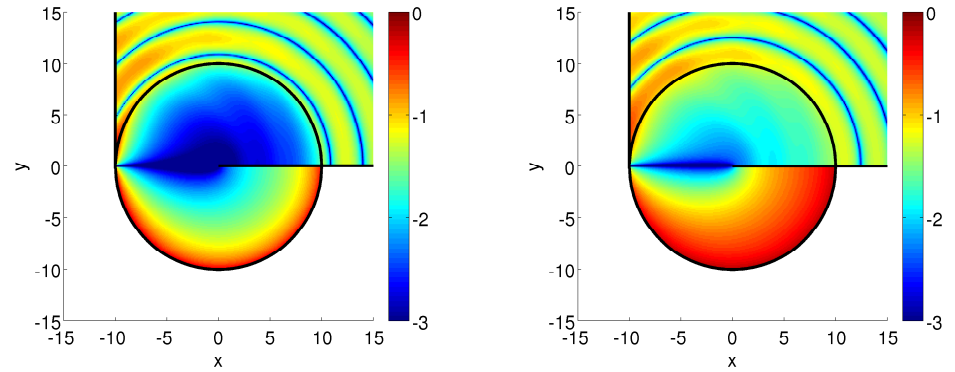

(a) $\log_{10}|\delta_{\mathrm{R}}|$ (b) $\log_{10}|\delta_{\mathrm{I}}|$

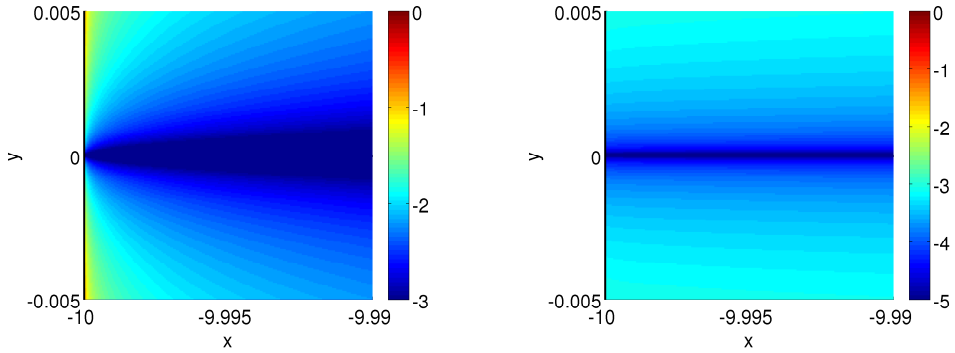

(c) $\log_{10}|\delta_{\mathrm{R}}|$ (d) $\log_{10}|\delta_{\mathrm{I}}|$

Figure 6: Logarithmic plots of $|\delta_{\mathrm{R}}|$ and $|\delta_{\mathrm{I}}|$ in the region behind the leading wavefront, for parameter values $t = 10$, $\theta_0 = 0^+$, $\omega = 1$, $c_0 = 1$. The magnified plots in (c) and (d) show the behaviour near the point $(-c_0 t, 0) = (-10, 0)$. Near this point the contours of $|\delta_{\mathrm{R}}|$ appear to be ellipsoidal, and the contours of $|\delta_{\mathrm{I}}|$ appear to be horizontal, as is predicted by the asymptotic analysis for the regime $\eta \ll \xi \ll 1$.

As in the point source case, to allow analytical progress in studying δ_{R} and δ_{I} it is convenient to rewrite (55) in a form similar to (44). We begin by decomposing Φ_{freq} into a sum of an incident field and a diffracted field, writing

$$\Phi_{\mathrm{freq}} = H(\pi - \theta) e^{-i\xi^{\mathrm{inc}}} - \operatorname{sgn}(\pi - \theta) \frac{e^{-i(\xi^{\mathrm{inc}} + \pi/4)}}{\sqrt{\pi}} \int_{\sqrt{\eta}}^{\infty} e^{is^2}\, ds, \qquad (56)$$

where $\eta = kr(1+\cos\theta)$ as before. We then apply the identity

$$\int_{\sqrt{\eta}}^{\infty} e^{is^2}\,ds = \frac{\sqrt{\eta}e^{i(\eta+\pi/4)}}{2\sqrt{\pi}} \int_0^{\infty} \frac{e^{is}}{\sqrt{s}(s+\eta)}\,ds, \qquad \eta > 0, \tag{57}$$

to obtain the representation

$$\Phi_{\text{freq}} = H(\pi-\theta)e^{-i\xi^{\text{inc}}} - \operatorname{sgn}(\pi-\theta)\frac{\sqrt{\eta}}{2\pi}\int_0^{\infty} \frac{e^{i(s-\xi)}}{\sqrt{s}(s+\eta)}\,ds, \tag{58}$$

where we have used the fact that $\xi + \eta = \xi^{\text{inc}}$. Comparing (44) and (58), we immediately note that for $\theta = \pi$ (i.e. along the shadow boundary) and $t > r/c_0$ we have

$$\Phi = \Phi_{\text{freq}} = \frac{1}{2}e^{-i\xi^{\text{inc}}}, \tag{59}$$

so that the frequency domain solution is immediately attained once the leading wavefront has arrived.

Away from $\theta = \pi$, the frequency domain solution is only attained asymptotically in time. With $\xi > 0$ we have

$$\delta\Phi = \pm\frac{\sqrt{\eta}}{2\pi}\int_{\xi}^{\infty} \frac{e^{i(s-\xi)}}{\sqrt{s}(s+\eta)}\,ds, \tag{60}$$

where $\pm$ denotes $-\operatorname{sgn}(\pi-\theta)$, and repeated integration by parts gives

$$\operatorname{Re}[\delta\Phi] \sim \pm\frac{\sqrt{\eta}(3\xi+\eta)}{4\pi\xi^{3/2}(\xi+\eta)^2}\left(1+O\left(\frac{1}{\xi^2}\right)\right), \qquad \xi\to\infty, \tag{61}$$

$$\operatorname{Im}[\delta\Phi] \sim \pm\frac{\sqrt{\eta}}{2\pi\sqrt{\xi}(\xi+\eta)}\left(1+O\left(\frac{1}{\xi^2}\right)\right), \qquad \xi\to\infty, \tag{62}$$

uniformly for all $\eta > 0$.

This implies that,

- for $\eta = O(1)$ but bounded away from zero (e.g. kr and θ fixed),

$$\delta_{\text{R}} = O\left(\frac{1}{\xi^{5/2}}\right), \qquad \xi\to\infty,\ \eta = O(1), \tag{63}$$

$$\delta_{\text{I}} = O\left(\frac{1}{\xi^{3/2}}\right), \qquad \xi\to\infty,\ \eta = O(1), \tag{64}$$

since $|\Phi_{\text{freq}}| = O(1)$ in this regime. Hence, as observed in Figure 4, the convergence of $\operatorname{Re}[\Phi]$ is indeed faster than that of $\operatorname{Im}[\Phi]$.

- For $\eta \ll 1$ (i.e. for observation points close to the shadow boundary) the asymptotic behaviour of the Fresnel integral (e.g. [6]) gives

$$\Phi_{\text{freq}} \sim \frac{e^{-i\xi}}{2}\left(1 \mp \frac{2e^{-i\pi/4}}{\sqrt{\pi}}\sqrt{\eta} + O\left(\eta\right)\right), \tag{65}$$

and combining (65) with (61) and (62) gives

$$\delta_{\text{R}} = O\left(\frac{\sqrt{\eta}}{\xi^{5/2}}\right), \qquad \xi \to \infty,\ \eta \ll 1, \tag{66}$$

$$\delta_{\text{I}} = O\left(\frac{\sqrt{\eta}}{\xi^{3/2}}\right), \qquad \xi \to \infty,\ \eta \ll 1. \tag{67}$$

The contours of δ_{R} and δ_{I} in this regime are, respectively, curves on which $\frac{\sqrt{\eta}}{\xi^{5/2}}$ and $\frac{\sqrt{\eta}}{\xi^{3/2}}$ are constant. See Figures 7(a) and 7(b) for an illustration.

In fact, as in the point source case, the assumption that $\eta \ll 1$ is enough to give convergence even when ξ is not large. For $\xi > \eta$ we can expand

$$\delta\Phi = \pm\frac{\sqrt{\eta}}{2\pi}\int_{\xi}^{\infty} \frac{e^{i(s-\xi)}}{s^{3/2}}\left(1 - \frac{\eta}{s} + \ldots\right) ds, \tag{68}$$

so that

$$\delta\Phi \sim \pm\frac{\sqrt{\eta}}{2\pi}\int_{\xi}^{\infty} \frac{e^{i(s-\xi)}}{s^{3/2}}\, ds, \qquad \eta \ll \xi. \tag{69}$$

In particular, when $\xi = O\left(1\right)$, but bounded away from zero, (11) and (12) hold with

$$\delta_{\text{R}}, \delta_{\text{I}} = O\left(\sqrt{\eta}\right), \qquad \xi = O\left(1\right),\ \eta \ll 1. \tag{70}$$

When $\xi \ll 1$, integration by parts gives

$$\text{Re}\left[\int_{\xi}^{\infty} \frac{e^{i(s-\xi)}}{s^{3/2}}\, ds\right] \sim \frac{2}{\sqrt{\xi}} + O\left(1\right), \qquad \xi \ll 1, \tag{71}$$

$$\text{Im}\left[\int_{\xi}^{\infty} \frac{e^{i(s-\xi)}}{s^{3/2}}\, ds\right] \sim \sqrt{2\pi} + O\left(\sqrt{\xi}\right), \qquad \xi \ll 1, \tag{72}$$

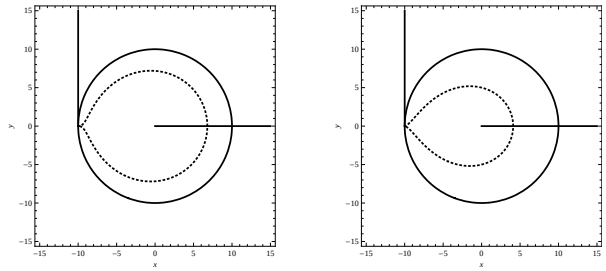

(a) $\varepsilon = \frac{\sqrt{\eta}}{\xi^{5/2}}$
(δ_{R}, $\xi \gg 1$, $\eta \ll 1$)

(b) $\varepsilon = \frac{\sqrt{\eta}}{\xi^{3/2}}$
(δ_{I}, $\xi \gg 1$, $\eta \ll 1$)

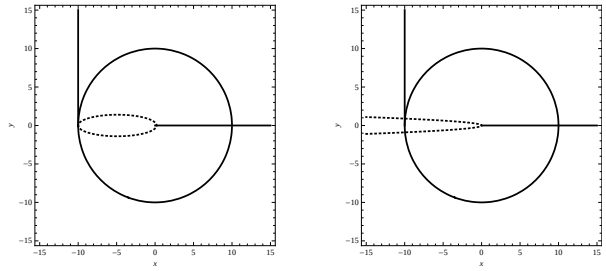

(c) $\varepsilon = \frac{\sqrt{\eta}}{\sqrt{\xi}}$
(δ_{R}, $\eta \ll \xi \ll 1$)

(d) $\varepsilon = \sqrt{\eta}$
(δ_{I}, $\eta \ll \xi \ll 1$)

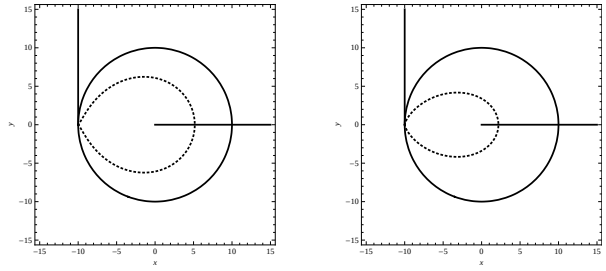

(e) $\varepsilon = \frac{\eta}{\xi^{5/2}}$
(δ_{R}, $1 \ll \eta \ll \xi$)

(f) $\varepsilon = \frac{\eta}{\xi^{3/2}}$
(δ_{I}, $1 \ll \eta \ll \xi$)

Figure 7: Illustration of contours of δ_{R}, δ_{I} as predicted by asymptotic analysis. For example, in (a) the plotted curve $\varepsilon = \frac{\sqrt{\eta}}{\xi^{5/2}}$ provides an illustration of a typical contour of δ_{R}, valid in the regime $\xi \gg 1$, $\eta \ll 1$. In each plot $\varepsilon = 0.2$. Other parameter values are $\theta_0 = 0^+$, $t = 10$, $\omega = 1$, $c_0 = 1$.

so that with $\eta \ll \xi \ll 1$, (11) and (12) hold with

$$\delta_{\mathrm{R}} = O\left(\frac{\sqrt{\eta}}{\sqrt{\xi}}\right), \qquad \eta \ll \xi \ll 1, \tag{73}$$

$$\delta_{\mathrm{I}} = O\left(\sqrt{\eta}\right), \qquad \eta \ll \xi \ll 1. \tag{74}$$

The contours of δ_{R} in this regime are curves on which ξ/η is constant, which, as we have already seen, are ellipses, whose axes all lie on the shadow boundary $\theta = \pi$. An illustration can be found in Figure 7(c). The ellipsoidal shape of the contours is clearly visible in Figure 6(c), which is a magnified version of Figure 6(a). The contours of δ_{I} are the curves of constant η, which are parabolae (as has already been remarked) with axis $\theta = \pi$ and focus at the origin. An illustration can be found in Figure 7(d). Near to the point $r = c_0 t$, $\theta = \pi$ they are approximately horizontal, as observed in Figure 6(d), which is a magnified version of Figure 6(b).

For completeness we remark that with $\eta \ll 1$, the estimate (74) (and hence (12)) holds even for $\xi = O(\eta)$, so that the horizontal contours described above go all the way to $\xi = 0$, as can be verified by combining the expansions (65) and (47).

- For $\eta \gg 1$ (i.e. for observation points far from the shadow boundary) the far-field behaviour (i.e. ray theory approximation) of the Fresnel integral (e.g. [6]) gives

$$\Phi_{\mathrm{freq}} \sim H(\pi - \theta) e^{-i\xi^{\mathrm{inc}}} \pm \frac{e^{-i(\xi - \pi/4)}}{2\sqrt{\pi}\sqrt{\eta}} \left(1 + O\left(\frac{1}{\eta}\right)\right), \quad \eta \gg 1, \tag{75}$$

so that

$$|\Phi_{\mathrm{freq}}| \sim \begin{cases} 1 & \eta \gg 1,\ \theta < \pi, \\ \dfrac{1}{2\sqrt{\pi}\sqrt{\eta}} & \eta \gg 1,\ \theta > \pi. \end{cases} \tag{76}$$

When $\theta > \pi$ (the NLOS region) the estimates (61) and (62) then give

$$\delta_{\mathrm{R}} = O\left(\frac{1}{\xi^{3/2}}\right), \qquad 1 \ll \eta,\ \xi = O(\eta), \tag{77}$$

$$\delta_{\mathrm{I}} = O\left(\frac{1}{\sqrt{\xi}}\right), \qquad 1 \ll \eta,\ \xi = O(\eta), \tag{78}$$

and

$$\delta_{\mathrm{R}} = O\left(\frac{\eta}{\xi^{5/2}}\right), \qquad 1 \ll \eta \ll \xi, \tag{79}$$

$$\delta_{\mathrm{I}} = O\left(\frac{\eta}{\xi^{3/2}}\right), \qquad 1 \ll \eta \ll \xi. \tag{80}$$

The contours of δ_{R} and δ_{I} in the regime $1 \ll \eta \ll \xi$ are, respectively, curves on which $\frac{\eta}{\xi^{5/2}}$ and $\frac{\eta}{\xi^{3/2}}$ are constant. See Figures 7(e) and 7(f) for an illustration.

When $\theta < \pi$ (the LOS region), however, (76) implies that we gain an extra factor of $1/\sqrt{\eta}$ in (77)-(80), giving closer agreement with the frequency domain solution than in the NLOS region. This asymmetry about $\theta = \pi$ is clearly visible in Figures 6(a) and 6(b).

In fact, in the LOS region the assumption that $\eta \gg 1$ allows us to prove (11) and (12) even when ξ is not large. With $\xi = O(1)$, but bounded away from zero, the same integrations by parts that lead to (61) and (62) can be used to show that

$$\mathrm{Re}[\delta\Phi],\, \mathrm{Im}[\delta\Phi] = O\left(\frac{1}{\sqrt{\eta}}\right), \qquad \eta \gg 1,\, \xi = O(1). \tag{81}$$

Moreover, the same estimates (81) hold for $\eta \gg 1$, $\xi \ll 1$, since by splitting the integral we have

$$\begin{aligned}\int_{\xi}^{\infty} \frac{e^{i(s-\xi)}}{\sqrt{s}(s+\eta)}\, ds &\sim \frac{1}{\eta}\int_{\xi}^{1} \frac{e^{i(s-\xi)}}{\sqrt{s}}\left(1 - \frac{s}{\eta} + \dots\right) ds + \int_{1}^{\infty} \frac{e^{i(s-\xi)}}{\sqrt{s}(s+\eta)}\, ds \\ &= O\left(\frac{1}{\eta}\right),\end{aligned} \tag{82}$$

where the estimate of the second term comes from applying the same procedure that led to (81) with $\xi = 1$. Thus in the LOS region $\theta < \pi$, (76) gives

$$\delta_{\mathrm{R}},\, \delta_{\mathrm{I}} = O\left(\frac{1}{\sqrt{\eta}}\right), \qquad \eta \gg 1,\, \xi = O(1). \tag{83}$$

Size of η	Size of ξ	Size of δ_{R}	Size of δ_{I}
$\eta \ll 1$	$\xi = O(\eta)$	No convergence	$O\left(\sqrt{\eta}\right)$
	$\eta \ll \xi = O(1)$	$O\left(\sqrt{\frac{\eta}{\xi}}\right)$	$O\left(\sqrt{\eta}\right)$
	$\xi \gg 1$	$O\left(\frac{\sqrt{\eta}}{\xi^{5/2}}\right)$	$O\left(\frac{\sqrt{\eta}}{\xi^{3/2}}\right)$
$\eta = O(1)$	$\xi \gg 1$	$O\left(\frac{1}{\xi^{5/2}}\right)$	$O\left(\frac{1}{\xi^{3/2}}\right)$
$\eta \gg 1$	$1 \ll \xi = O(\eta)$	$O\left(\frac{1}{\xi^{3/2}}\right)$	$O\left(\frac{1}{\sqrt{\xi}}\right)$
$\theta > \pi$ (NLOS)	$\xi \gg \eta$	$O\left(\frac{\eta}{\xi^{5/2}}\right)$	$O\left(\frac{\eta}{\xi^{3/2}}\right)$
$\eta \gg 1$	$\xi = O(1)$	$O\left(\frac{1}{\sqrt{\eta}}\right)$	$O\left(\frac{1}{\sqrt{\eta}}\right)$
$\pi < \theta$ (LOS)	$1 \ll \xi = O(\eta)$	$O\left(\frac{1}{\sqrt{\eta}\xi^{3/2}}\right)$	$O\left(\frac{1}{\sqrt{\eta}\sqrt{\xi}}\right)$
	$\xi \gg \eta$	$O\left(\frac{\sqrt{\eta}}{\xi^{5/2}}\right)$	$O\left(\frac{\sqrt{\eta}}{\xi^{3/2}}\right)$

Table 1: Summary of convergence results in the diffracted region $r < c_0 t$ ($\xi > 0$).

- Finally, for completeness we remark that in the region $\theta < \pi$, $r > c_0 t$, $x > -c_0 t$ (i.e. after the arrival of the incident wavefront but before the arrival of the diffracted wavefront), we have

$$\delta\Phi = -\frac{\sqrt{\eta}}{2\pi} \int_0^\infty \frac{e^{i(s-\xi)}}{\sqrt{s}(s+\eta)}\, ds. \tag{84}$$

  If $\eta \gg 1$ then (81) (and hence (83)) holds, so that the frequency domain solution provides the leading order behaviour, even though the diffracted wavefront has yet to arrive.

The results of this section are summarised in Table 1.

3.3. The case $\theta_0 \neq 0$

In this section we briefly consider the general case in which the plane wave is incident from an arbitrary angle $0 < \theta_0 < \pi$. When $\pi/2 \leq \theta_0 < \pi$, (3) is replaced by

$$\Phi = G(t + (r/c_0)\cos(\theta - \theta_0)), \qquad t < 0, \tag{85}$$

and when $0 < \theta_0 < \pi/2$ a reflected wave is also present initially, so that

$$\Phi = \sum_{\pm} H(\pi - (\theta \pm \theta_0))G(t + (r/c_0)\cos(\theta \pm \theta_0)), \qquad t < 0, \tag{86}$$

where $\sum_{\pm}$ indicates that the sum of the + and − terms should be taken.

In both cases the time-harmonic solution Φ_{freq} is the sum of two terms, each associated with one of the two shadow boundaries $\theta = \pi \pm \theta_0$. Each term is of the form (58), but with θ replaced by $\theta \pm \theta_0$, and ξ^{inc}, η replaced by $\xi_\pm = \omega t + kr\cos(\theta \pm \theta_0)$, $\eta_\pm = kr(1 + \cos(\theta \pm \theta_0))$, respectively. Similarly, Φ is the sum of two terms of the form (44). Plots of Φ and Φ_{freq} for the cases $\theta_0 = \pi/3$ and $\theta_0 = 2\pi/3$ are presented in Figures 8(a)-(d) and 9(a)-(d), respectively, and corresponding plots of the relative errors δ_R and δ_I can be found in Figures 8(e)-(f) and 9(e)-(f).

Generalising the analysis of the previous section to the case $\theta_0 \neq 0$ is straightforward, and we do not present the details here. There are, however, some important qualitative differences in the way that the time-dependent solution converges to the frequency domain solution, as compared to the case $\theta_0 = 0$, which we now remark upon.

First, we note that the frequency domain solution is not instantaneously attained along either of the shadow boundaries $\theta = \pi \pm \theta_0$. This is because along either shadow boundary, although one of the two terms making up Φ converges instantaneously, the other does not. However, the convergence is immediate along the line $\theta = \pi$ (i.e. the continuation of the half-line into $x < 0$). Indeed, once the incident wavefront has arrived we have

$$\Phi = \Phi_{\text{freq}} = e^{-i\omega(t-(r/c_0)\cos\theta_0)}, \qquad \theta = \pi, \;\; t > \frac{r\cos\theta_0}{c_0}. \tag{87}$$

Second, we remark on the 'tongue-like' features observed in the reflected region $0 < \theta < |\pi - \theta_0|$ in the relative error plots in Figures 8(e)-(f) and 9(e)-(f) . These are due to the effect of interference between the incident and reflected components of Φ_{freq}. Along the lines

$$y = \frac{(n + 1/2)\pi}{k\sin\theta_0}, \qquad n = 0, 1, 2, \ldots, \tag{88}$$

the incident and reflected components of Φ_{freq} cancel exactly, so that Φ_{freq} comprises only a (small) diffracted component in the far field. In the vicinity

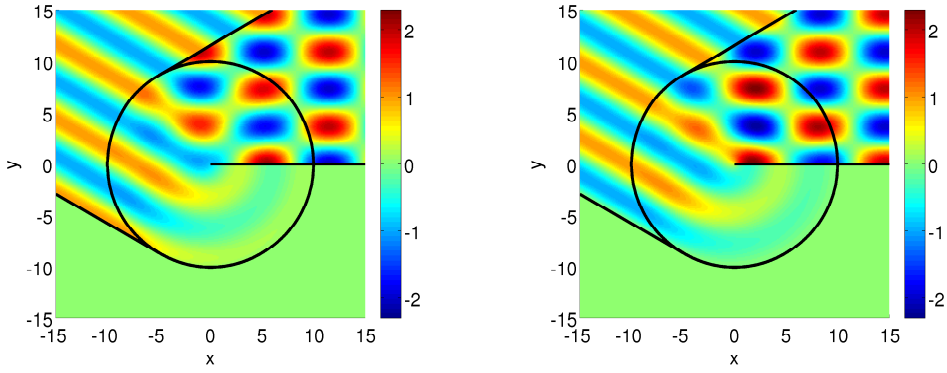

(a) $\mathrm{Re}[\Phi]$ (b) $\mathrm{Im}[\Phi]$

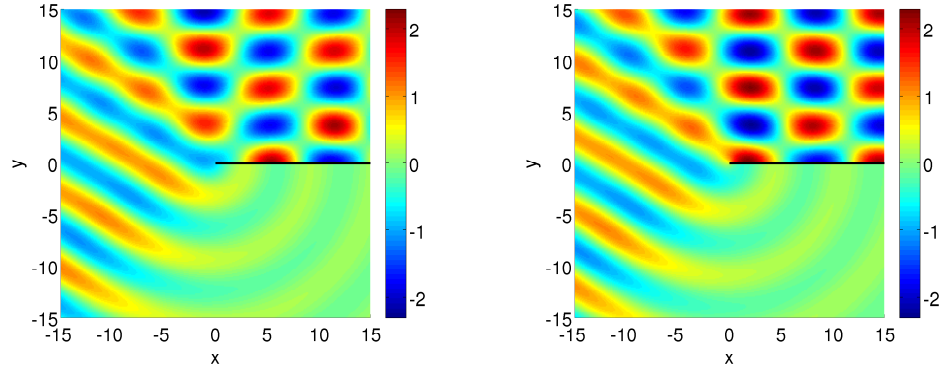

(c) $\mathrm{Re}[\Phi_{\mathrm{freq}}]$ (d) $\mathrm{Im}[\Phi_{\mathrm{freq}}]$

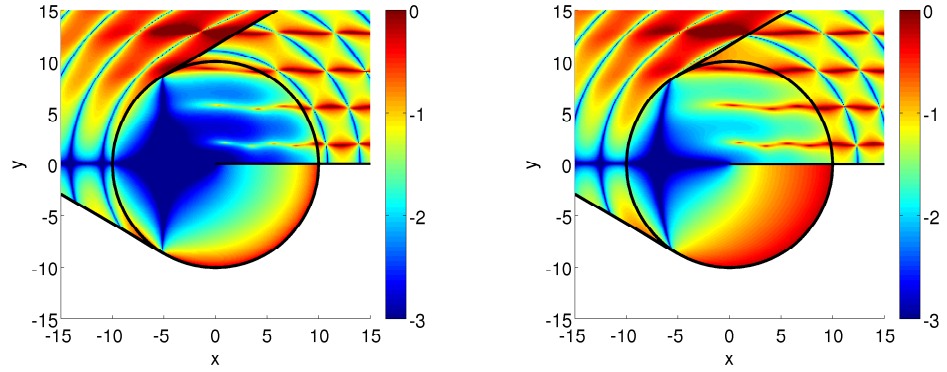

(e) $\log_{10}|\delta_{\mathrm{R}}|$ (f) $\log_{10}|\delta_{\mathrm{I}}|$

Figure 8: Plots of Φ, Φ_{freq}, $|\delta_{\mathrm{R}}|$ and $|\delta_{\mathrm{I}}|$ for $t = 10$, $\theta_0 = \pi/3$, $\omega = 1$, $c_0 = 1$.

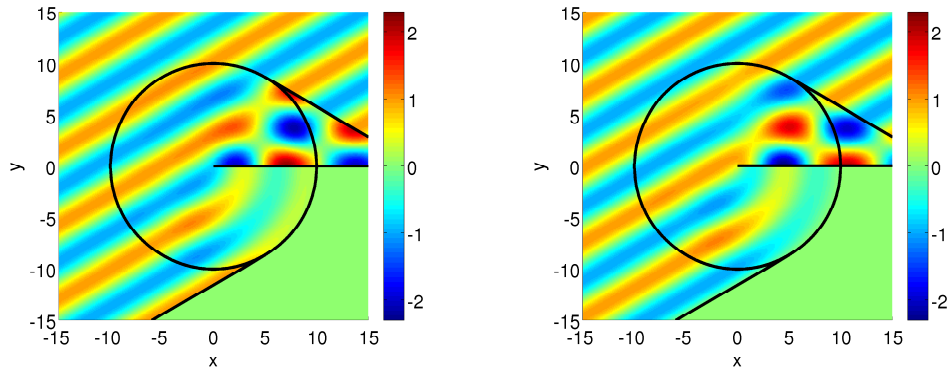

(a) $\mathrm{Re}[\Phi]$

(b) $\mathrm{Im}[\Phi]$

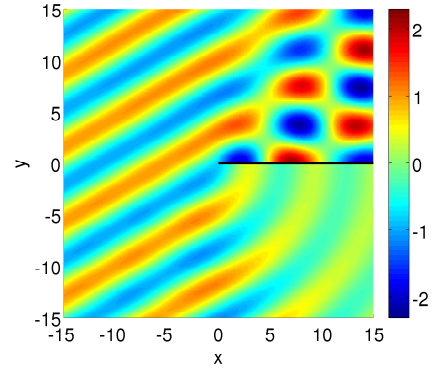

(c) $\mathrm{Re}[\Phi_{\mathrm{freq}}]$

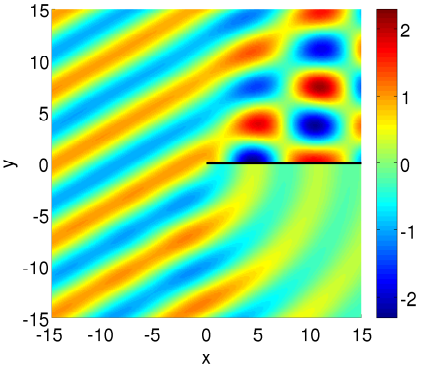

(d) $\mathrm{Im}[\Phi_{\mathrm{freq}}]$

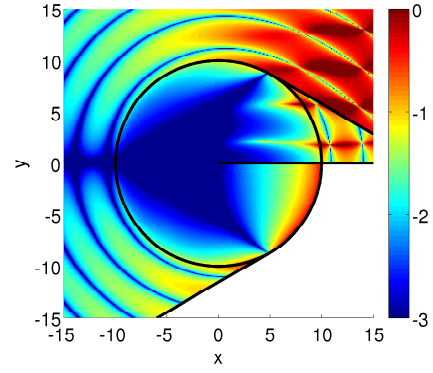

(e) $\log_{10}|\delta_{\mathrm{R}}|$

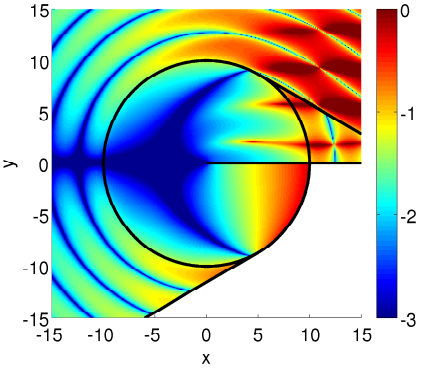

(f) $\log_{10}|\delta_{\mathrm{I}}|$

Figure 9: Plots of Φ, Φ_{freq}, $|\delta_{\mathrm{R}}|$ and $|\delta_{\mathrm{I}}|$ for $t = 10$, $\theta_0 = 2\pi/3$, $\omega = 1$, $c_0 = 1$.

of these lines, δ_R and δ_I are therefore similar in magnitude to what they are in the corresponding part of the NLOS region (i.e. at angle $2\pi - \theta$). Away from these lines, $\Phi_{\text{freq}} = O(1)$, so that, as was found to be the case for $\theta_0 = 0$ (see the remark after (77)-(80)), δ_R and δ_I are smaller in the LOS region than in the corresponding part of the NLOS region.

4. Concluding remarks

In this paper we have considered two two-dimensional scalar wave propagation problems in which a time-harmonic wave is switched on instantaneously, namely a point source in free space, and the diffraction of a plane wave by a half-line, on which a rigid (Neumann) boundary condition is imposed. In both cases, we have been able to show how the pulse-like behaviour on the leading wavefront tends to the time-harmonic behaviour of the corresponding frequency domain solution on a suitable timescale.

Interestingly, we have found that the manner in which the wave is switched on is of great importance in determining the rate of convergence to the frequency domain solution, with a stronger singularity on the leading wavefront giving rise to faster convergence. In the case of diffraction by a half-line, the rate of convergence has also been shown to depend strongly on the observation point. In particular, at grazing incidence the frequency domain solution is attained along the shadow boundary immediately after the arrival of the leading wavefront.

Interesting areas for further work could be to study

(i) distributed sources, and in particular when the length scale associated with the source, L say, is such that $\omega L/c_0 \gg 1$. In such a situation the frequency domain solution could be approximated using ray theory.

(ii) three-dimensional problems. When a time-harmonic point source is switched on in three dimensions, the frequency domain solution is attained instantaneously behind the leading wavefront. Also, our analysis of switched-on plane waves incident on a half-line in two dimensions can be trivially generalised to three-dimensional incidence on a half-plane, the diffracted wavefront now being conical. We might conjecture that it is only in the presence of boundaries that are equivalent to a finite collection of image sources that the frequency domain solution is attained in finite time.

5. Acknowledgements

D. P. Hewett acknowledges the support of the EPSRC and Dstl (MOD research programme, contract RD023-2985).

References

[1] R. N. Buchal, The approach to steady state of solutions of exterior boundary value problems for the wave equation, J. Math. Mech. 12 (2) (1963), 225–234.

[2] C. S. Morawetz, The limiting amplitude principle, Comm. Pure and App. Math. 15 (3) (1962), 349–361.

[3] C. S. Morawetz, The limiting amplitude principle for arbitrary finite bodies, Comm. Pure and App. Math. 18 (1-2) (1965), 183–189.

[4] A. I. Komech and A. E. Merzon, Limiting amplitude principle in the scattering by wedges, Math. Meth. Appl. Sci. 29 (2006), 1147-1185.

[5] A. T. de Hoop, A modification of Cagniard's method for solving seismic pulse problems, App. Sci. Research B8 (1960), 349-356.

[6] M. Abramowitz and I. A. Stegun, Handbook of Mathematical Functions, United States Department of Commerce, 1964.

[7] F. G. Friedlander, Sound Pulses, Cambridge University Press, Cambridge, 1958.

[8] J. B. Keller and A. Blank, Diffraction and reflection of pulses by wedges and corners, Comm. Pure and App. Math. 4 (1) (1951), 75–94.

[9] D. P. Hewett, Sound propagation in an urban environment, DPhil thesis, University of Oxford, 2010.

[10] D. S. Jones, Acoustic and Electromagnetic Waves, Oxford University Press, USA, 1989.